

Plaque rupture in coronary atherosclerosis is associated with increased plaque structural stress

Charis Costopoulos MD¹, Yuan Huang PhD, MD², Adam J. Brown MD, PhD¹, Patrick A. Calvert MD, PhD⁴, Stephen P. Hoole MD⁴, Nick E. J. West MD⁴, Jonathan H. Gillard MD², Zhongzhao Teng PhD^{2,3}, Martin R. Bennett, MD, PhD¹

¹Division of Cardiovascular Medicine and Departments of ²Radiology and ³Engineering, University of Cambridge, UK

⁴Department of Interventional Cardiology, Papworth Hospital NHS Trust, UK

Address for correspondence:

Prof. Martin R. Bennett

Division of Cardiovascular Medicine

University of Cambridge

Level 6, ACCI, Addenbrooke's Hospital,

Cambridge, CB2 0QQ, UK

Tel.: +44 122 333 1504 Fax: +44 122 333 1505

E-mail: mrb@mole.bio.cam.ac.uk

Word Count: 4500

Figures: 7

Tables: 3

Dr Zhongzhao Teng, Department of Radiology, University of Cambridge

Box 218 Cambridge Biomedical Campus, Hills Road

Cambridge, CB2 0QQ, UK

Tel: +44 (0)1223 746447 Fax: +44 (0)1223 330915

Email: zt215@cam.ac.uk

Short Title: Coronary Plaque Structural Stress And Rupture

Author email addresses:

Charis Costopoulos: charis.costopoulos.cardiology@gmail.com; Yuan Huang: yh288@cam.ac.uk; Adam J. Brown: adam.brown7@nhs.net; Patrick A. Calvert: paddy@doctors.org.uk; Stephen P. Hoole: s.hoole@nhs.net; Nick E.J. West: nick.west1@nhs.net; Jonathan H. Gillard: jhg21@cam.ac.uk; Zhongzhao Teng: zt215@cam.ac.uk; Martin R. Bennett: mrb@mole.bio.cam.ac.uk

Funding Sources

This work was supported by British Heart Foundation Grants CH/20000003/12800, FS/13/33/30168, and FS/15/26/31441, Heart Research UK Grant RG2638/14/16, and MRC Confidence in Concepts award, and the NIHR Cambridge Biomedical Research Centre.

Disclosures: None

ABSTRACT

Background: Plaque rupture is the commonest cause of myocardial infarction, occurring particularly in higher-risk lesions such as fibroatheromas. However, prospective virtual-histology intravascular ultrasound (VH-IVUS) studies indicate that <10% higher-risk plaques cause clinical events over 3-years, indicating that other factors also determine plaque rupture. Plaque rupture occurs when plaque structural stress (PSS) exceeds its mechanical strength; however, the determinants of PSS and its association with proven plaque rupture sites are not known.

Objectives: To identify the determinants of PSS, and the relationship between PSS and plaque rupture.

Methods: We analyzed plaque structure and composition in 4,053 VH-IVUS frames from 32 fibroatheromas with rupture from the VIVA study and 32 fibroatheromas without rupture on optical coherence tomography from a stable angina cohort. Mechanical loading in the periluminal region was estimated by calculating maximum principal plaque structural stress (PSS) by finite element analysis.

Results: PSS increased with increasing lumen area ($r=0.46$; $p=0.001$), lumen eccentricity ($r=0.32$; $p=0.001$), and necrotic core $\geq 10\%$ ($r=0.12$; $p=0.001$), but reduced when dense calcium $\geq 10\%$ ($r=-0.12$; $p=0.001$). Ruptured fibroatheromas showed higher PSS (133 [90-191] vs. 104kPa [75-142]; $p=0.002$) and variation in PSS (55 [37-75] vs. 43kPa [34-59]; $p=0.002$) than non-ruptured fibroatheromas, with rupture primarily occurring either proximal or immediately adjacent to the minimal luminal area (87.5 vs. 12.5%; $p=0.001$). PSS was

higher in segments proximal to the rupture site (143 [101-200] vs. 120kPa [78-180]; $p=0.001$) vs. distal segments, associated with increased necrotic core (19.1 [11-29] vs. 14.3% [8-23]; $p=0.001$) but reduced fibrous/fibrofatty tissue (63.6 [46-78] vs. 72.7% [54-86]; $p=0.001$). PSS $>135\text{kPa}$ was a good predictor of rupture in higher-risk regions.

Conclusions: PSS is determined by plaque composition, plaque architecture, and lumen geometry. PSS and PSS variability are increased in plaques with rupture, particularly at proximal segments. Incorporating PSS into plaque assessment may improve identification of rupture-prone plaques.

Key words: atherosclerosis, vulnerable plaque, coronary disease

CONDENSED ABSTRACT

Plaque rupture is believed to occur when plaque structural stress (PSS) exceeds the material strength of the fibrous cap; however, the determinants of PSS and its relationship to proven rupture sites are unknown. We examined PSS in 4,053 VH-IVUS frames from 32 fibroatheromas with rupture and 32 fibroatheromas without rupture. PSS increased with increasing lumen area, lumen eccentricity, and necrotic core $\geq 10\%$, but reduced when dense calcium $\geq 10\%$. Ruptured fibroatheromas showed higher PSS than non-ruptured fibroatheromas. PSS $> 135\text{kPa}$ was a good predictor of rupture in higher-risk regions. Incorporating PSS into plaque assessment may therefore improve identification of rupture-prone plaques.

LIST OF ABBREVIATIONS

FA=fibroatheroma

FEA = finite element analysis

MACE = major adverse cardiovascular events

MLA = minimal luminal area

OCT = optical coherence tomography

PB = plaque burden

PSS = plaque structural stress

VH-IVUS = virtual-histology intravascular ultrasound

VH-FA = virtual-histology fibroatheroma

VH-TCFA = virtual-histology thin-cap fibroatheroma

Introduction

Rupture of a coronary plaque is the precipitating event in the majority of myocardial infarctions (MI)¹. Post-mortem² and *in vivo* intravascular studies^{3,4} identify fibroatheromas (FAs), and in particular thin-cap fibroatheromas (TCFAs), as the most common predisposing lesion. TCFAs are widespread in human coronary artery disease, including asymptomatic individuals and those with stable and unstable syndromes³. However, the incidence of major adverse cardiovascular events (MACE) associated with TCFAs identified by virtual-histology intravascular ultrasound (VH-IVUS) is <10% over ~3-years follow-up^{3,4}, suggesting that factors other than plaque and lumen size or plaque phenotype are important in determining plaque rupture.

Plaque rupture occurs when intra-plaque stress exceeds the material strength of the overlying fibrous cap; increased plaque structural stress (PSS) is therefore a potential mechanism that determines rupture of a higher-risk lesion. PSS can be calculated through an engineering technique known as finite element analysis (FEA), which approximates a solution to the equations of mechanical equilibrium by considering tissue material properties, plaque geometry and local hemodynamic forces. Histological and VH-IVUS studies have identified necrotic core size, fibrous cap thickness and the presence of microcalcification as important determinants of PSS⁵⁻⁷. PSS has also been shown to be increased in patients presenting with acute coronary syndromes (ACS) vs. stable symptoms⁸. However, the determinants of PSS and its relationship to plaque rupture sites *in vivo* in human coronary arteries are not known. We sought to identify the parameters that determine PSS and variations in PSS across ruptured and non-ruptured FAs identified using VH-IVUS, to determine whether plaque stress is increased at plaque rupture sites, and whether incorporating PSS into plaque assessment

improves identification of rupture-prone plaques.

METHODS

Study Design

All plaques from the VH-IVUS in Vulnerable Atherosclerosis (VIVA) study with evidence of rupture (n=32) on grey-scale IVUS (GS-IVUS)³ were included in the study. To compare ruptured vs. non-ruptured plaques, we performed optical coherence tomography (OCT) prior to VH-IVUS imaging on a separately recruited cohort of 40 patients with stable angina admitted for elective percutaneous coronary intervention (PCI)(ref 11/EE/0277). Lesions from this cohort were included only where there was no evidence of plaque rupture or erosion on VH-IVUS and OCT. As spontaneous rupture occurred only in FAs in VIVA, only VH-IVUS-identified FAs (VH-FAs) were included in the non-ruptured group, yielding 32 plaques from 32 patients (**Fig. 1 and Online Methods**).

VH-IVUS and OCT Analysis

VH-IVUS data were acquired with 20 MHz Eagle-Eye catheters (Volcano Corporation, Rancho, Cordova) using motorized pullback at 0.5mm/s. OCT data were acquired with Dragonfly C7 catheters (St. Jude Medical, St. Paul, US) using an automated pullback at 20mm/sec. Plaque classification, identification of rupture (**Fig. 2**) and characterization of rupture location along the plaque length (**Online Fig. 1**) were performed as previously described (**Online Methods**). VH-IVUS plaque frames which demonstrated rupture were not included in the final analysis for ruptured plaques as the extreme luminal eccentricity due to rupture at these frames would make PSS calculations unreliable.

Biomechanical Analysis

Plaques underwent dynamic 2D FEA simulations as previously described⁸ (**Online Methods**). Maximum principal stress was used to indicate the critical mechanical conditions within the structure, referred as PSS. A 65 μ m layer of fibrous tissue was introduced during mesh generation to account for the limited axial resolution of VH-IVUS to detect a fibrous cap between lumen and necrotic core/dense calcium. Examples of PSS band plots with their corresponding VH-IVUS images are shown in **Fig. 3**.

Statistical Analysis

Data were assessed for normality using the Shapiro-Wilk test. Normally distributed variables are presented as mean (SD) and compared using unpaired t-test, and non-normal outcomes presented as median (Q1-Q3) using Mann-Whitney U tests. Correlations between variables are expressed as Spearman correlation coefficients for non-normally distributed data.

Multivariable regression modeling was performed to determine the independent predictors of PSS with purposeful selection of covariates in the cohort of VH-IVUS frames of plaque burden (PB) \geq 70% and necrotic core $>$ 10% as these have been linked with future events^{3,4,9}.

Variables associated on univariate analysis ($p < 0.10$) were included in the multivariable model-building process. As each plaque had multiple VH-IVUS slices, a linear mixed model was used to compare groups using a random effect for plaque and fixed effects for group. All calculations were two-tailed with $p < 0.05$ considered statistically significant. Statistical analyses were performed both in SPSS 19.0.0 (SPSS Inc., IBM Computing, US) and R 2.10.1 (The R Foundation for Statistical Computing).

RESULTS

Baseline Patient and VH-IVUS Demographics

We analyzed PSS in patients who had spontaneous plaque rupture on GS-IVUS from the VIVA study (n=25 patients, n=32 plaques), compared to patients undergoing elective PCI where plaque rupture was excluded both by GS-IVUS and OCT (n=32 patients, n=32 plaques)(**Figs. 1 and 2**). Patient demographics were similar between the ruptured and non-ruptured groups (**Table 1**), with no differences in procedural systolic (129.9 vs. 123.8mmHg; p=0.31) or diastolic blood pressure (66.2 vs. 65.6mmHg, p=0.85).

There were no significant differences in plaque classification between the 2 groups, with VH-TCFA being the predominant plaque type accounting for rupture or undergoing PCI for stable angina (91 vs. 75%; p=0.14)(**Table 2**). PB was lower in ruptured plaques (59.5 vs. 63.5%; p=0.01), but minimal luminal area (MLA) and multiple components of plaque composition (% fibrous/fibrofatty tissue, necrotic core, dense calcium) were similar. Patient demographics and plaque composition for the cohort of patients with only VH-TCFAs also did not differ significantly between the groups (**Online Tables 1 and 2**).

Determinants of PSS in Virtual-histology-defined Fibroatheromas

We used FEA to estimate both the amount and location of PSS in both ruptured and non-ruptured plaques, and the plaque and vessel determinants of PSS. Both luminal area and luminal eccentricity correlated positively with PSS (r=0.46; p=0.001 and r=0.32; p=0.001, respectively), whereas a negative correlation was observed with PB (r=-0.23; p=0.001)(**Table 3**). A positive correlation with PSS was also observed when frames with necrotic core $\geq 10\%$ were considered (r=0.12; p=0.001)(**Table 3**), indicating that necrotic core only affects PSS when its contribution exceeds 10%. In contrast, dense calcium $\geq 10\%$ and maximum arc of

dense calcium demonstrated negative correlations with PSS ($r=-0.12$ and -0.13 respectively, both $p=0.001$)(**Table 3**), suggesting that calcification offers a plaque ‘shielding’ effect when present in significant amounts. Fibrous/fibrofatty tissue was associated with PSS only when increasingly confluent, with no correlation seen with % tissue ($r=0.02$; $p=0.13$)(**Table 3**) but a negative correlation observed with maximum arc ($r=-0.19$; $p=0.001$). PSS varies throughout the cardiac cycle, with highest and lowest values corresponding to systolic and diastolic pressures. This cyclical stretching and relaxation may be particularly important to induce plaque ‘fatigue’. Indeed, PSS variability during the cardiac cycle was correlated with broadly similar parameters to peak PSS (**Online Table 3**), although fibrous/fibrofatty tissue (%) was negatively correlated and maximum arc of dense calcium was not correlated.

Our data show that PSS is determined by a number of factors, which differ depending on plaque type and extent of disease. We therefore undertook regression analysis to assess whether individual plaque parameters could predict PSS in FAs. Although weak associations were observed between luminal area, plaque eccentricity, plaque burden (PB)(**Figs. 4A-4C**) and individual plaque components (**Figs. 5A-5F**) there were no factors that could individually determine PSS.

PSS is likely to have the greatest clinical impact when high stress occurs in a higher risk region. We therefore used multivariable regression modeling to identify independent determinants of PSS in higher-risk segments. Luminal area, PB, % necrotic core, % dense calcium, fibrous/fibrofatty tissue arc, necrotic core arc, calcium arc and lumen eccentricity were all included in the final model. A significant regression equation was observed ($F(8,677) = 82.1$; $p=0.001$), with an R^2 of 0.49 ($R^2_{\text{adjusted}}=0.49$). Luminal area ($\beta=0.53$; $p=0.001$), necrotic core arc ($\beta=0.10$; $p=0.04$), and lumen eccentricity ($\beta=0.32$; $p=0.001$) were

independent positive predictors of PSS, and calcium arc ($\beta=-0.12$; $p=0.003$) and fibrous/fibrofatty tissue arc ($\beta=-0.25$; $p=0.001$) were independent negative predictors of PSS.

PSS and Plaque Rupture

Although our data indicates that PSS is associated with plaque features considered to promote rupture, the relationship between PSS and plaques that demonstrate actual rupture is unclear. We therefore examined PSS in plaques with GS-IVUS evidence of rupture compared to plaques where rupture was excluded on OCT (**Fig. 2**). Compared to non-ruptured FAs, ruptured FAs showed higher PSS (133 [90-191] vs. 104kPa [75-142]; $p=0.002$)(**Online Fig. 2A**), and this was also seen when either proximal (143 [101-200] vs. 108kPa [78-150]; $p=0.001$) or distal segments (120 [78-180] vs. 101kPa [71-138]; $p=0.01$) were specifically examined (**Fig. 6A**). Similarly, compared to non-ruptured FAs, ruptured FAs showed greater variation in PSS between systole and diastole (55 [37-75] vs. 43kPa [34-59]; $p=0.02$)(**Online Fig. 2B**), and this was also seen when proximal [57 [38-74] vs. 45kPa [35-60]; $p=0.04$) or distal 54 [34-75] vs. 42kPa [32-57]; $p=0.01$) segments were examined (**Fig. 6B**).

Certain VH-IVUS features have been associated with a higher MACE risk, notably VH-TCFA, $PB \geq 70\%$ and $MLA \leq 4\text{mm}^2$, and further increased by combinations of these features^{3,4,9}. PSS and variation in PSS were significantly higher in ruptured vs. non-ruptured VH-TCFAs (**Figs. 6C and 6D**), and again this was seen in both proximal and distal segments. Similarly, both PSS and variation in PSS were higher in plaques that were VH-TCFAs with $PB \geq 70\%$ (PSS: 137 [95-190] vs. 80kPa [57-113]; $p=0.001$; variation in PSS: 54 [38-74] vs. 37kPa [28-49]; $p=0.001$)(**Figs. 6E and 6F**), but similar between ruptured and non-ruptured VH-TCFAs when $MLA \leq 4\text{mm}^2$ (PSS: 88 [62-134] vs. 83kPa [59-122]; $p=0.51$; variation in PSS: 52 [33-72] vs. 38kPa [30-52]; $p=0.08$)(**Figs. 6E and 6F**). We also performed receiver

operating characteristic curve analysis to assess the ability of PSS to predict plaque rupture (**Figs. 7A-7C**). Inclusion of PSS significantly improved the ability of the combination of VH-FA+PB $\geq 70\%$ to identify plaque rupture (**Fig. 7C**). An optimal PSS cut-off of 135kPa was identified for this cohort, associated with good sensitivity (72.1%), specificity (83.3%), positive predictive (78.3%), and negative predictive (78.1%) values.

Location of Plaque Rupture and Distribution of PSS in Ruptured Plaques

The frequency of plaque rupture varies between the main coronary arteries, with left anterior descending (LAD) and right coronary (RCA) FAs being more prone to rupture than left circumflex artery (LCx) FAs, a similar pattern to coronary artery occlusion leading to ST-elevation MI^{10,11}. In addition, FAs in the proximal segments are particularly at risk^{10,12}. We found that ruptures were more common in the RCA (59.3%), followed by LAD (40.1%) and LCx (15.6%), and 80% of ruptures occurred in the first 33mm of the artery. Rupture occurred primarily either in the proximal or middle (MLA and peri-MLA) plaque segments (87.5 vs. 12.5%; $p=0.001$) in agreement with previously published data¹³.

PSS and variations in PSS differed markedly over short distances both within the same plaque and between plaques, irrespective of whether these ruptured (**Online Fig. 3**). We therefore examined whether differences in PSS could explain the location of rupture, and whether this reflected differences in plaque composition. Both PSS (143 [101-200] vs. 120kPa [78-180]; $p=0.001$) and variation in PSS (57 [38-74] vs. 54kPa [34-75]; $p=0.02$) were higher in the segments proximal to rupture sites (**Figs. 6A and 6B and Online Fig. 4**) vs. distal sites. Proximal plaque segments comprised less fibrous/fibrofatty tissue (63.6 [46-78] vs. 72.7% [54-86]; $p=0.001$) but greater necrotic core (19.1 [11-29] vs. 14.3% [8-23]; $p=0.001$) and dense calcium (13.2 [6-25] vs. 10.1% [3-23]; $p=0.001$) than distal sites. Necrotic core arc (43

[27-66] vs. 34° [21-53]; p=0.001), calcium arc (47 [23-81] vs. 32° [14-66]; p=0.001) and fibrous/fibrofatty arc (144 [96-216] vs. 131° [89-191]); p=0.001) were all also increased in the proximal segments. PSS in the LAD/RCA arteries was higher compared to the LCx (136 [93-195] vs. 90kPa [66-130]; p=0.01) with no differences noted in PSS variation between the 2 vessel groups (54 [36-74] vs. 64kPa [45-80]; p=0.18).

Discussion

Plaque rupture is the precipitating event in the majority of MIs, and is thought to occur at sites of plaque weakness¹. PSS is a potential trigger of rupture, with rupture occurring when PSS exceeds the mechanical strength of the overlying fibrous cap. *Ex vivo* carotid studies have shown that peak circumferential stress is highest at areas of rupture⁵, which has been confirmed by subsequent *in vivo* MRI studies, despite the limited capability of MRI to accurately identify plaque components¹⁴. However, estimation of PSS in human coronary plaques *in vivo* is more challenging. Recently we demonstrated that PSS estimated from VH-IVUS is higher in culprit plaques of patients presenting with ACS than stable symptoms⁸. However, patients with ACS have a variety of plaque substrates and circumstances that account for their presentation. The current study examined the relationship between VH-IVUS-derived PSS and proven plaque rupture compared to plaques of similar classification in which rupture was excluded.

PSS and Plaque Architecture

We find that PSS in coronary FAs is determined by multiple parameters, including plaque size, composition, and luminal geometry. PSS is increased by luminal area and eccentricity, but reduced by PB. PSS is increased when necrotic core is $\geq 10\%$, but reduced when dense calcium $\geq 10\%$. However, these relationships are complex, and none of the individual plaque parameters examined were able to independently determine PSS, even when considered only in higher-risk regions. The proximal segment of plaques also showed differences in composition that increase PSS compared with distal segments, including increased % necrotic core and decreased % fibrous/fibrofatty tissue. The observation that luminal area correlates positively with PSS indicates that plaques causing mild or moderate stenosis may be under greater stress and therefore more prone to rupture, compared to plaques that cause greater

lumen stenosis. This is consistent with serial coronary angiography studies that demonstrate that vessel occlusion, largely due to plaque rupture, often occurs at sites with less severe stenosis¹⁵⁻¹⁷. Collectively, these results suggest that PSS is influenced by factors other than overall plaque composition, such as the spatial relationship between adjacent components and the lumen, parameters that are ignored by current classification systems of plaque vulnerability.

PSS and Plaque Rupture

We find that plaque rupture clusters in the RCA and LAD, and close to the coronary ostia, especially in the LAD^{10,12}, similar to post-mortem studies¹². We also find that proximal or peri-MLA plaque segments are more prone to rupture¹³, which are sites expected to have higher PSS due to their larger luminal area, in accordance with Laplace's law ($\sigma=Pr/h$ where σ =circumferential stress, P =intra-arterial pressure r =vessel radius and h =vessel wall thickness). Plaque segments proximal to the rupture site also showed higher PSS, and this was associated with significant differences in plaque composition. More importantly, we demonstrate that both PSS and variation in PSS are higher in ruptured than non-ruptured plaques, which was also seen when only VH-TCFAs or $PB \geq 70\%$ were examined. This suggests that rupture occurs in a subset of higher-risk plaques already under high stress, when either a further increase in PSS occurs or large variations in PSS promote cap fatigue¹⁸, or both. PSS in the vicinity of 135kPa appears to be particularly important, a cut-off that is associated with good positive and negative predictive values in identifying plaques that demonstrate rupture. The finding that PSS did not differ between ruptured vs. non-ruptured plaques at sites of $MLA \leq 4mm^2$ is consistent with results from the ATHEROREMO-IVUS (European Collaborative Project on Inflammation and Vascular Wall Remodeling in

Atherosclerosis – Intravascular Ultrasound) study, where $MLA \leq 4\text{mm}^2$ did not predict future MACE⁹.

Study Limitations

Our study has some limitations. First, although we demonstrated that ruptured plaques were associated with higher PSS, we cannot calculate exact PSS levels at the precise rupture site. Second, as PSS calculations are dependent on the resolution of VH-IVUS and its ability to accurately identify plaque components, PSS derived from VH-IVUS has the same limitations. However VH-IVUS is the only intravascular imaging modality with a) prospective clinical data correlating MACE with particular plaque phenotypes, b) automatic component identification and segmentation, thus eliminating an important source of human error and c) sufficient penetration to image the whole plaque, which is important for accurate PSS calculations. Third, our study consists of 2 cohorts that were obtained at different time points. However, OCT was not performed in the VIVA study, but was necessary in the unruptured patient population to exclude rupture, thereby ensuring that the non-ruptured group truly consisted of intact plaques.

Conclusions

We demonstrate that VH-IVUS-based PSS is dependent on components of plaque composition and plaque and lumen architecture that are also associated with plaque vulnerability and rupture, thereby indirectly linking PSS to plaque rupture. More importantly, PSS is higher in plaques with proven rupture, particularly in segments proximal to the rupture site, which have increased necrotic core. $PSS > 135\text{kPa}$ appears to be a good predictor of rupture in higher-risk regions. Our results suggest that incorporation of PSS calculations into

coronary plaque assessment may improve our ability to identify those plaques that proceed to rupture and clinical events.

Perspectives

Translational Outlook: Plaque rupture is the precipitating event in the majority of myocardial infarctions. However, in prospective VH-IVUS studies <10% of high-risk plaques were responsible for cardiac events over 3 years, suggesting that other factors play a role in this process. Plaque structural stress (PSS) can be estimated from VH-IVUS images, and is proposed as a mechanism that determines rupture in high-risk regions. Incorporation of PSS into assessment of coronary atherosclerotic plaques may improve our ability to identify those that cause clinical events.

References:

1. Davies MJ, Thomas A. Thrombosis and acute coronary-artery lesions in sudden cardiac ischemic death. *N Engl J Med* 1984; **310**(18): 1137-40.
2. Virmani R, Burke AP, Kolodgie FD, Farb A. Pathology of the thin-cap fibroatheroma: a type of vulnerable plaque. *J Interv Cardiol* 2003; **16**(3): 267-72.
3. Calvert PA, Obaid DR, O'Sullivan M, et al. Association between IVUS findings and adverse outcomes in patients with coronary artery disease: the VIVA (VH-IVUS in Vulnerable Atherosclerosis) Study. *JACC Cardiovasc Imaging* 2011; **4**(8): 894-901.
4. Stone GW, Maehara A, Lansky AJ, et al. A prospective natural-history study of coronary atherosclerosis. *N Engl J Med* 2011; **364**(3): 226-35.
5. Richardson PD, Davies MJ, Born GV. Influence of plaque configuration and stress distribution on fissuring of coronary atherosclerotic plaques. *Lancet* 1989; **2**(8669): 941-4.
6. Loree HM, Kamm RD, Stringfellow RG, Lee RT. Effects of fibrous cap thickness on peak circumferential stress in model atherosclerotic vessels. *Circ Res* 1992; **71**(4): 850-8.
7. Huang H, Virmani R, Younis H, Burke AP, Kamm RD, Lee RT. The impact of calcification on the biomechanical stability of atherosclerotic plaques. *Circulation* 2001; **103**(8): 1051-6.
8. Teng Z, Brown AJ, Calvert PA, et al. Coronary Plaque Structural Stress Is Associated With Plaque Composition and Subtype and Higher in Acute Coronary Syndrome: The BEACON I (Biomechanical Evaluation of Atheromatous Coronary Arteries) Study. *Circ Cardiovasc Imaging* 2014; **7**(3): 461-70.
9. Cheng JM, Garcia-Garcia HM, de Boer SP, et al. In vivo detection of high-risk coronary plaques by radiofrequency intravascular ultrasound and cardiovascular outcome: results of the ATHEROREMO-IVUS study. *European Heart Journal* 2014; **35**(10): 639-47.

10. Hong MK, Mintz GS, Lee CW, et al. The site of plaque rupture in native coronary arteries: a three-vessel intravascular ultrasound analysis. *J Am Coll Cardiol* 2005; **46**(2): 261-5.
11. Wang JC, Normand SL, Mauri L, Kuntz RE. Coronary artery spatial distribution of acute myocardial infarction occlusions. *Circulation* 2004; **110**(3): 278-84.
12. Cheruvu PK, Finn AV, Gardner C, et al. Frequency and distribution of thin-cap fibroatheroma and ruptured plaques in human coronary arteries: a pathologic study. *J Am Coll Cardiol* 2007; **50**(10): 940-9.
13. Fukumoto Y, Hiro T, Fujii T, et al. Localized elevation of shear stress is related to coronary plaque rupture: a 3-dimensional intravascular ultrasound study with in-vivo color mapping of shear stress distribution. *J Am Coll Cardiol* 2008; **51**(6): 645-50.
14. Tang D, Teng Z, Canton G, et al. Sites of rupture in human atherosclerotic carotid plaques are associated with high structural stresses: an in vivo MRI-based 3D fluid-structure interaction study. *Stroke* 2009; **40**(10): 3258-63.
15. Little WC, Constantinescu M, Applegate RJ, et al. Can coronary angiography predict the site of a subsequent myocardial infarction in patients with mild-to-moderate coronary artery disease? *Circulation* 1988; **78**(5 Pt 1): 1157-66.
16. Ambrose JA, Tannenbaum MA, Alexopoulos D, et al. Angiographic progression of coronary artery disease and the development of myocardial infarction. *J Am Coll Cardiol* 1988; **12**(1): 56-62.
17. Giroud D, Li JM, Urban P, Meier B, Rutishauer W. Relation of the site of acute myocardial infarction to the most severe coronary arterial stenosis at prior angiography. *Am J Cardiol* 1992; **69**(8): 729-32.
18. Teng Z, Sadat U, Huang Y, et al. In vivo MRI-based 3D mechanical stress-strain profiles of carotid plaques with juxtaluminal plaque haemorrhage: an exploratory study for

the mechanism of subsequent cerebrovascular events. *Eur J Vasc Endovasc Surg* 2011; **42**(4): 427-33.

Figure Legends

Figure 1. Schematic representation of patient and plaque populations included in the study

FEA=finite element analysis; OCT=optical coherence tomography; VH-FA=virtual-histology fibroatheroma; VIVA=VH-IVUS in Vulnerable Atherosclerosis study.

Figure 2. Identification of plaque rupture using grey-scale intravascular ultrasound and optical coherence tomography

(A-B) Grey-scale IVUS images of spontaneous plaque rupture (*). **(C)** OCT image showing evidence of rupture (*). **(D)** Thin-cap fibroatheroma (arrow) as identified by OCT with no evidence of rupture or erosion. **(E)** Longitudinal IVUS reconstruction of a coronary artery with evidence of plaque rupture (proximal (*A'*), rupture site (*B'*) and distal (*C'*) segments). IVUS=intravascular ultrasound; OCT=optical coherence tomography.

Figure 3. Illustrative examples for stepwise calculation of plaque structural stress from virtual-histology intravascular ultrasound through finite element analysis

(A and D) VH-IVUS images showing necrotic core (red), dense calcium (white), fibrofatty tissue (light green) and fibrous (green). **(B and E)** Reconstructed plaque geometry and segmented plaque components used for FEA. **(C and F)** PSS band plots identifying regions with high stress concentration (arrows indicate areas of high stress at the plaque/lumen boundary). FEA=finite element analysis; PSS=plaque structural stress; VH-IVUS=virtual-histology ultrasound.

Figure 4. Indices of vessel geometry and plaque structural stress

(A-C) Regression curves illustrating best-fit relationships between PSS and (A) luminal area, (B) luminal eccentricity or (C) plaque burden. PSS=plaque structural stress.

Figure 5. Effect of plaque components on plaque structural stress

(A-F) Regression curves illustrating best-fit relationships between PSS and (A) necrotic core (%), (B) maximal arc of necrotic core (°), (C) dense calcium (%), (D) maximal arc of dense calcium (°), (E) fibrous/fibrofatty tissue (%), and (F) maximal arc of fibrous/fibrofatty tissue (°). PSS=plaque structural stress.

Figure 6. Plaque structural stress and variation in PSS in virtual-histology fibroatheromas with and without rupture

(A and B) PSS and variation in PSS in the proximal and distal segments of VH-FAs with and without plaque rupture. (C and D) PSS and variation in PSS in the proximal and distal segments of VH-TCFAs with and without PR. (E and F) PSS and variation in PSS in VH-TCFAs with $PB \geq 70\%$ or $MLA \leq 4\text{mm}^2$ with and without PR. MLA=minimal luminal area; PR=plaque rupture; PSS=plaque structural stress; VH-FA=virtual-histology fibroatheroma; VH-TCFA=virtual-histology thin-cap fibroatheroma.

Figure 7. Receiver operating characteristic curves illustrating the discriminatory power of PSS to identify plaque rupture

(A) ROC curve for PSS in VH-FA (B) ROC curve for PSS in VH-FA+ $MLA \leq 4\text{mm}^2$, and (C) ROC curve for PSS in VH-FA+ $PB \geq 70\%$. AUC=area under the curve; CI=confidence interval; MLA=minimal lumen area; PB=plaque burden; ROC=receiver operating characteristic; VH-FA=virtual-histology fibroatheroma.

Table 1. Demographics of patients with ruptured and non-ruptured plaques

Characteristic	Ruptured (n=25)	Non-ruptured (n=32)	p-value
Age, y	61.4 (10.4)	64.0 (10.1)	0.46
Male, n (%)	20 (80)	29 (90.6)	0.25
Diabetes mellitus, n (%)	2 (8)	6 (18.8)	0.25
Hypertension, n (%)	9 (36)	10 (31.3)	0.71
Hypercholesterolemia, n (%)	8 (32)	6 (18.8)	0.25
Smoker, n (%)	8 (32)	6 (18.8)	0.25
Family history of CAD, n (%)	14 (56)	12 (37.5)	0.43
Procedural blood pressure			
Systolic blood pressure, mm Hg	129.9 (25.1)	123.8 (18.9)	0.31
Diastolic blood pressure, mm Hg	66.2 (8.5)	65.6 (9.3)	0.85
Total cholesterol, mmol/L	3.57 (0.88)	3.83 (0.97)	0.35
LDL cholesterol, mmol/L	2.37 (0.84)	2.68 (0.98)	0.25
HDL cholesterol, mmol/L	1.21 (0.47)	1.15 (0.26)	0.60
Total cholesterol:HDL ratio	3.34 (1.62)	3.51 (1.47)	0.72
Creatinine, mg/DL	85.6 (17.5)	94.9 (22.5)	0.11
hsCRP, mg/L	11.6 (28.9)	5.36 (8.8)	0.26

Data are shown as mean (SD) or n (%). CAD=coronary artery disease; hsCRP=high-sensitivity C-reactive protein; HDL=high-density lipoprotein; LDL=low-density lipoprotein; MI=myocardial infarction

Characteristic	Ruptured (n=32)	Non-Ruptured (n=32)	p-value
VH-TCFA, n (%)	29 (90.6)	24 (75)	0.14
Plaque burden, n (%)	58.2 (6.8)	63.5 (4.8)	0.01
Minimal luminal area $\leq 4\text{mm}^2$, n (%)	30 (93.8)	32 (100)	0.14
Fibrous/fibrofatty, n (%)	60.8 (54-70)	67.5(60-75)	0.10
Necrotic core, (%)	18.9 (15-27)	18.3 (14-23)	0.46
Dense calcium, (%)	15.8 (11-24)	14.1 (7-22)	0.33
<i>Plaque characteristics at frame level</i>			
Fibrous/fibrofatty, (%)	67.5 (50-82)	69.1 (50-84)	0.44
Necrotic core, (%)	16.5 (9-26)	15.6 (9-26)	0.18
Dense calcium, (%)	11.8 (4-24)	11.2 (4-25)	0.58
Maximum arc of fibrous/fibrofatty tissue, (°)	137.3 (93-205)	140.3 (94-205)	0.24
Maximum arc of necrotic core, (°)	38.5 (25-60)	37.1 (22-57)	0.18
Maximum arc of dense calcium, (°)	40.5(18-76)	37.1 (18-64)	0.12
Lumen eccentricity	0.51 (0.4-0.6)	0.5 (0.4-0.6)	0.38

Data shown are n (%), mean (SD) or median (Q1–Q3). VH-IVUS=virtual-histology intravascular ultrasound; VH-TCFA=virtual-histology thin-cap fibroatheroma

Table 2. VH-IVUS parameters of ruptured and non-ruptured plaques

Characteristic	Correlation coefficient (r)	p-value	Table 3. Correlation coefficients between PSS and VH-IVUS parameters
Luminal area, (mm ²)	0.46	0.001	
Plaque burden, (%)	-0.23	0.001	
Lumen eccentricity	0.32	0.001	
Necrotic core ≥10, (%)	0.12	0.001	
Maximum arc of necrotic core, (°)	0.01	0.70	
Dense calcium ≥10, (%)	-0.12	0.001	
Maximum arc of dense calcium, (°)	-0.13	0.001	
Fibrous/fibrofatty tissue, (%)	0.02	0.13	
Maximum arc of fibrous/fibrofatty tissue, (°)	-0.19	0.001	

PSS=plaque structural stress; VH-IVUS=virtual-histology intravascular ultrasound

eters

Figure 1

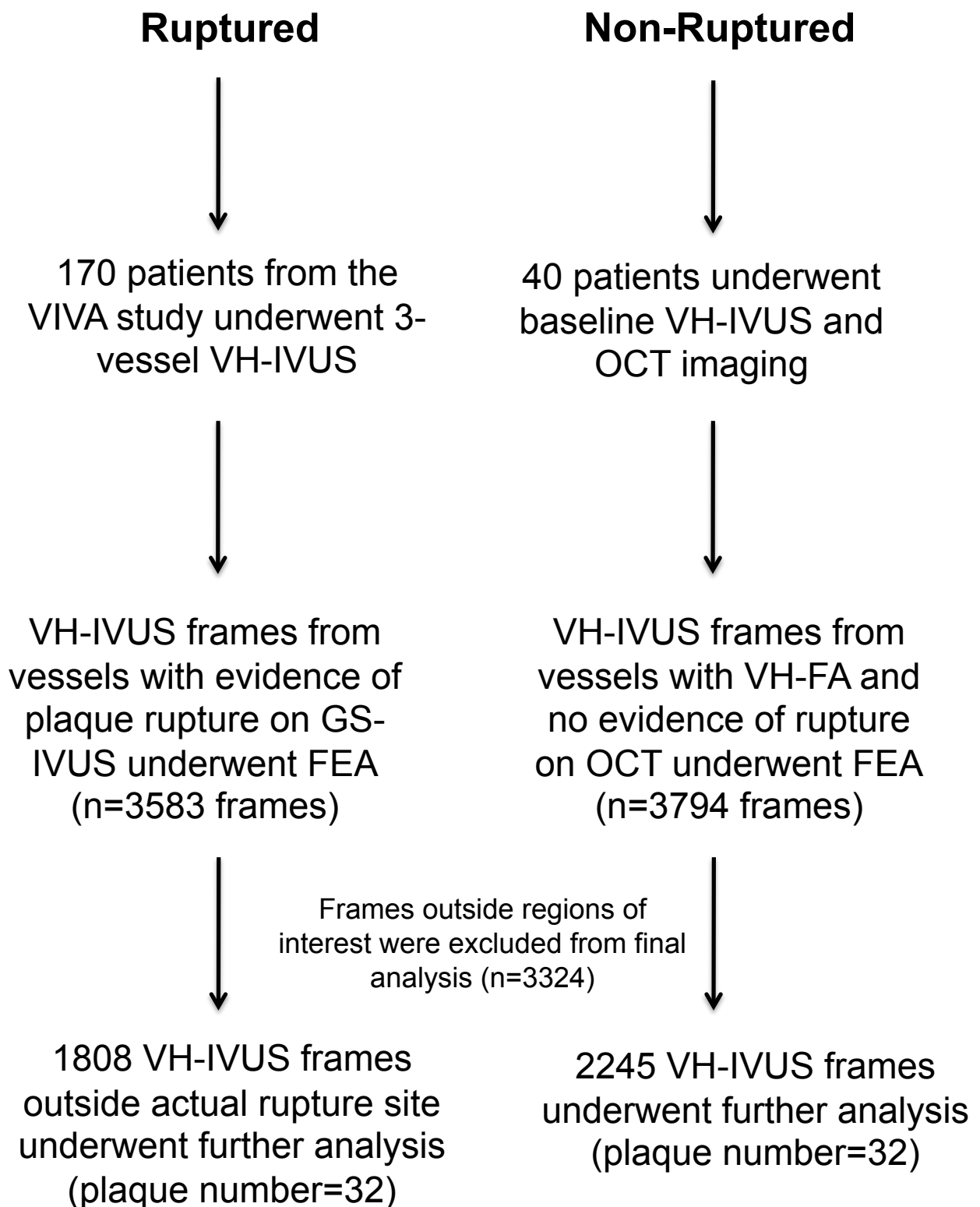


Figure 1. Schematic representation of patient and plaque populations included in the study

FEA=finite element analysis; OCT=optical coherence tomography; VH-FA=virtual-histology fibroatheroma; VIVA=VH-IVUS in Vulnerable Atherosclerosis study.

Figure 2

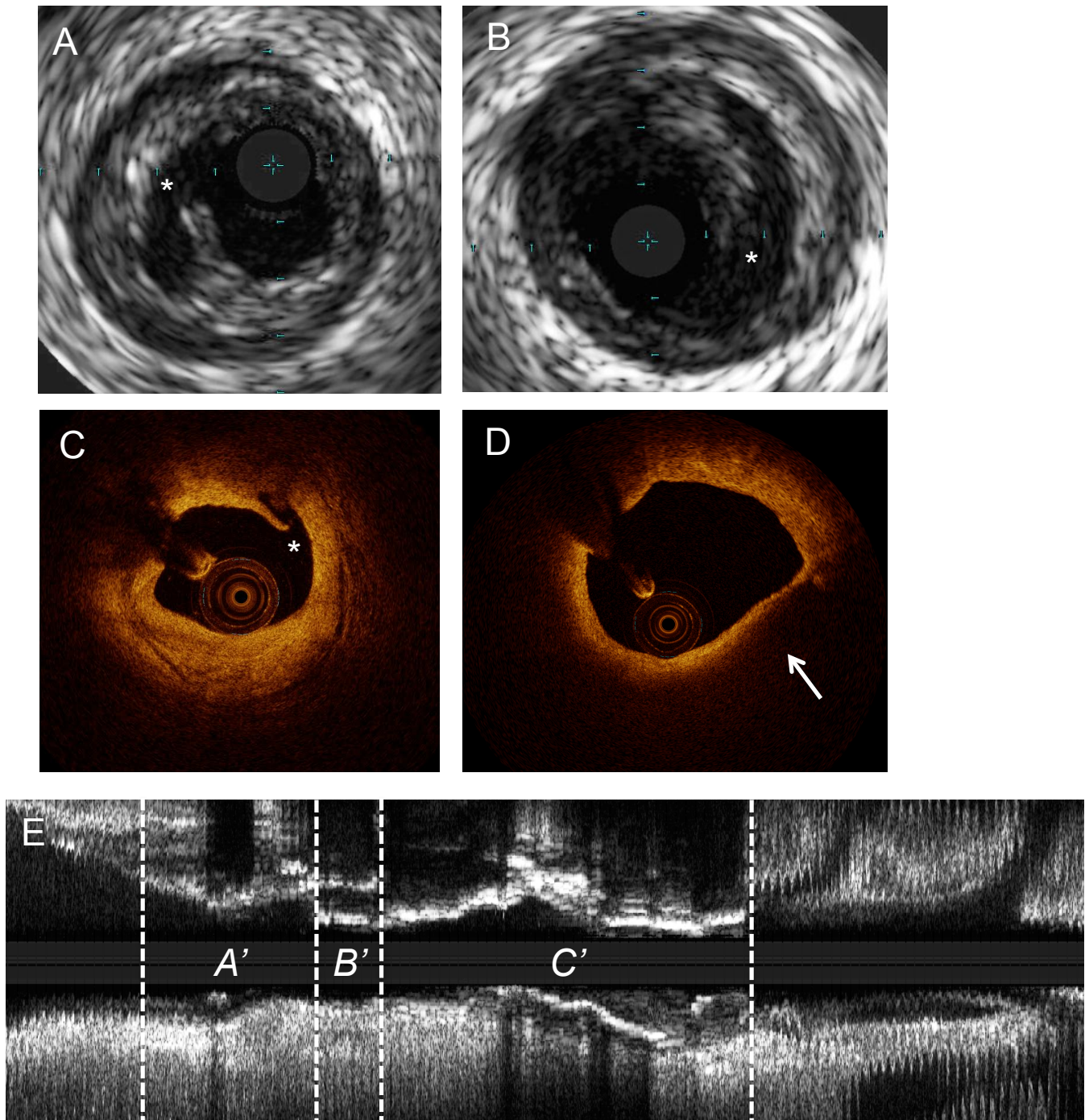


Figure 2. Identification of plaque rupture using grey-scale intravascular ultrasound and optical coherence tomography

(A-B) Grey-scale IVUS images of spontaneous plaque rupture (*). **(C)** OCT image showing evidence of rupture (*). **(D)** Thin-cap fibroatheroma (arrow) as identified by OCT with no evidence of rupture or erosion. **(E)** Longitudinal IVUS reconstruction of a coronary artery with evidence of plaque rupture (proximal (A'), rupture site (B') and distal (C') segments). IVUS=intravascular ultrasound; OCT=optical coherence tomography.

Figure 3

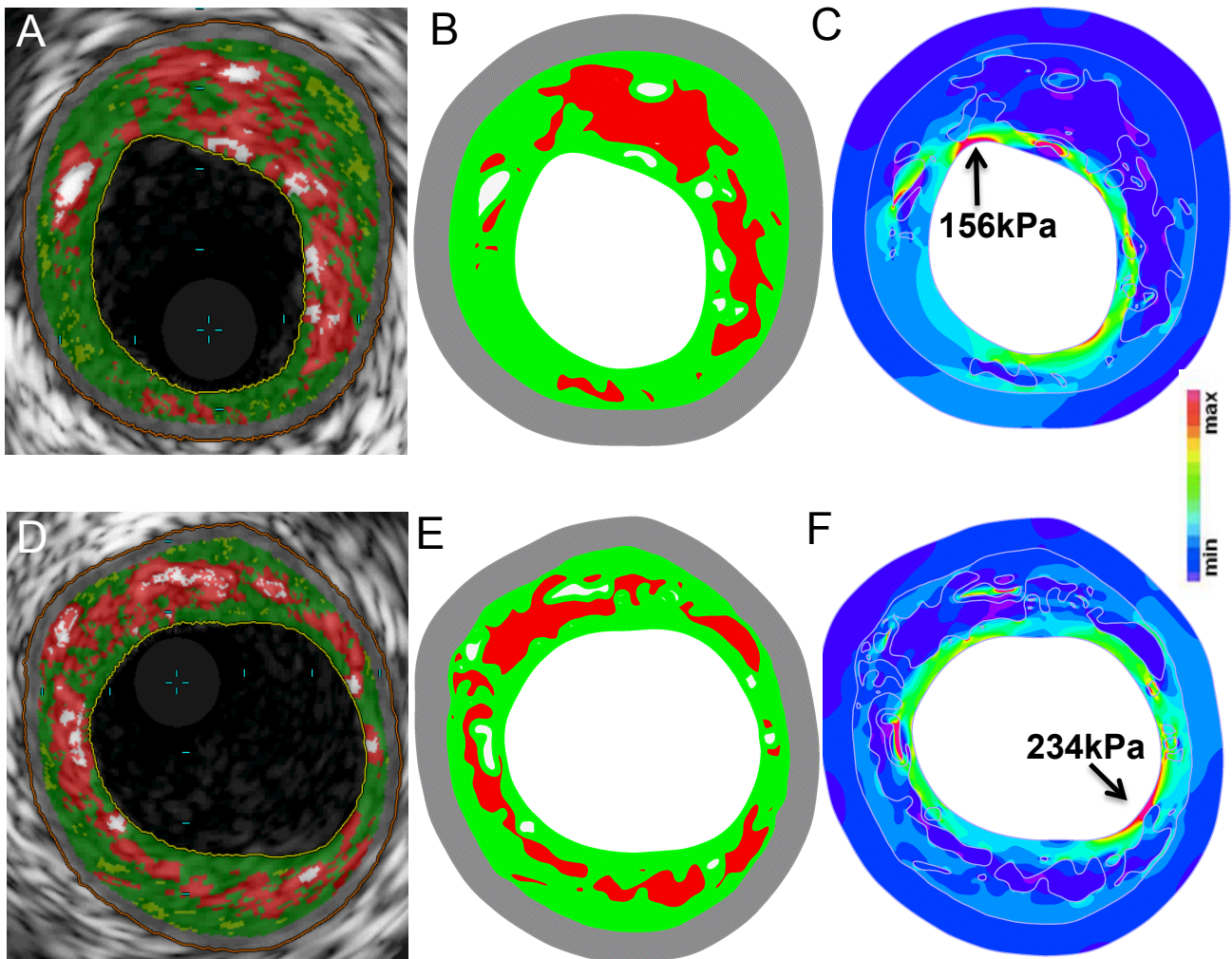


Figure 3. Illustrative examples for stepwise calculation of plaque structural stress from virtual-histology intravascular ultrasound through finite element analysis (A and D) VH-IVUS images showing necrotic core (red), dense calcium (white), fibrofatty tissue (light green) and fibrous (green). (B and E) Reconstructed plaque geometry and segmented plaque components used for FEA. (C and F) PSS band plots identifying regions with high stress concentration (arrows indicate areas of high stress at the plaque/lumen boundary). FEA=finite element analysis; PSS=plaque structural stress; VH-IVUS=virtual-histology ultrasound.

Figure 4

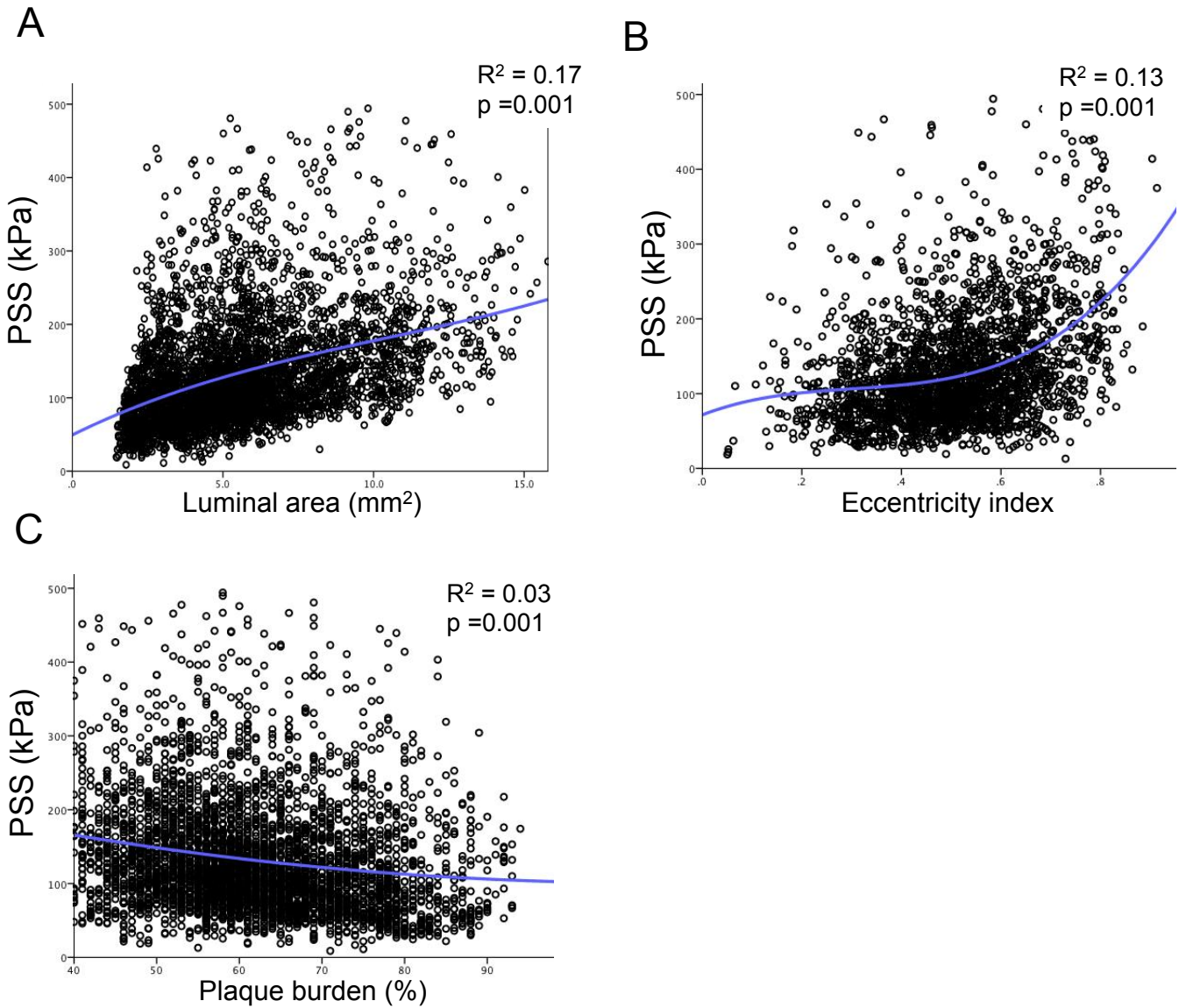


Figure 4. Indices of vessel geometry and plaque structural stress
(A-C) Regression curves illustrating best-fit relationships between PSS and (A) luminal area, (B) luminal eccentricity or (C) plaque burden. PSS=plaque structural stress.

Figure 5

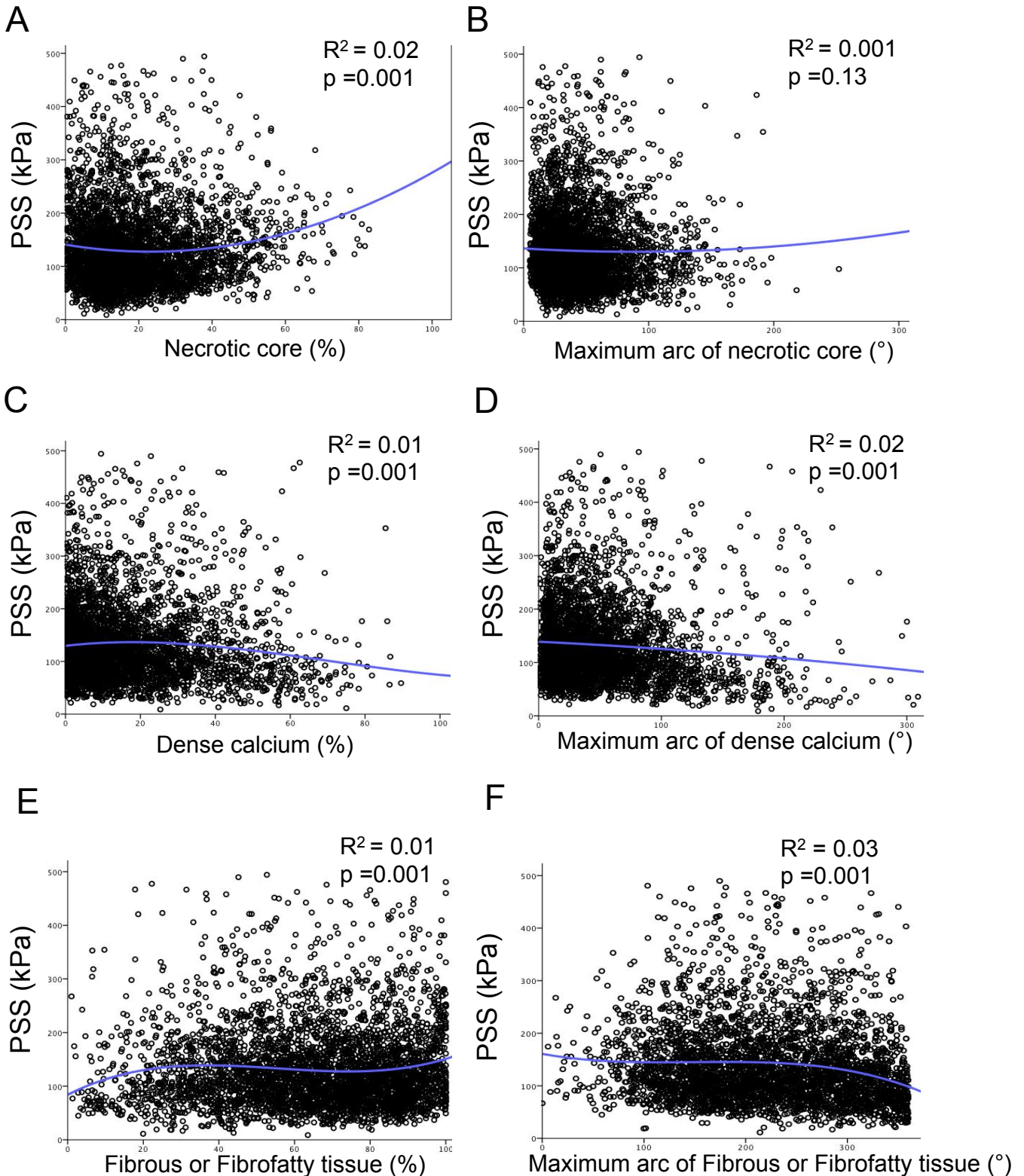


Figure 5. Effect of plaque components on plaque structural stress

(A-F) Regression curves illustrating best-fit relationships between PSS and (A) necrotic core (%), (B) maximal arc of necrotic core ($^\circ$), (C) dense calcium (%), (D) maximal arc of dense calcium ($^\circ$), (E) fibrous/fibrofatty tissue (%), and (F) maximal arc of fibrous/fibrofatty tissue ($^\circ$). PSS=plaque structural stress.

Figure 6

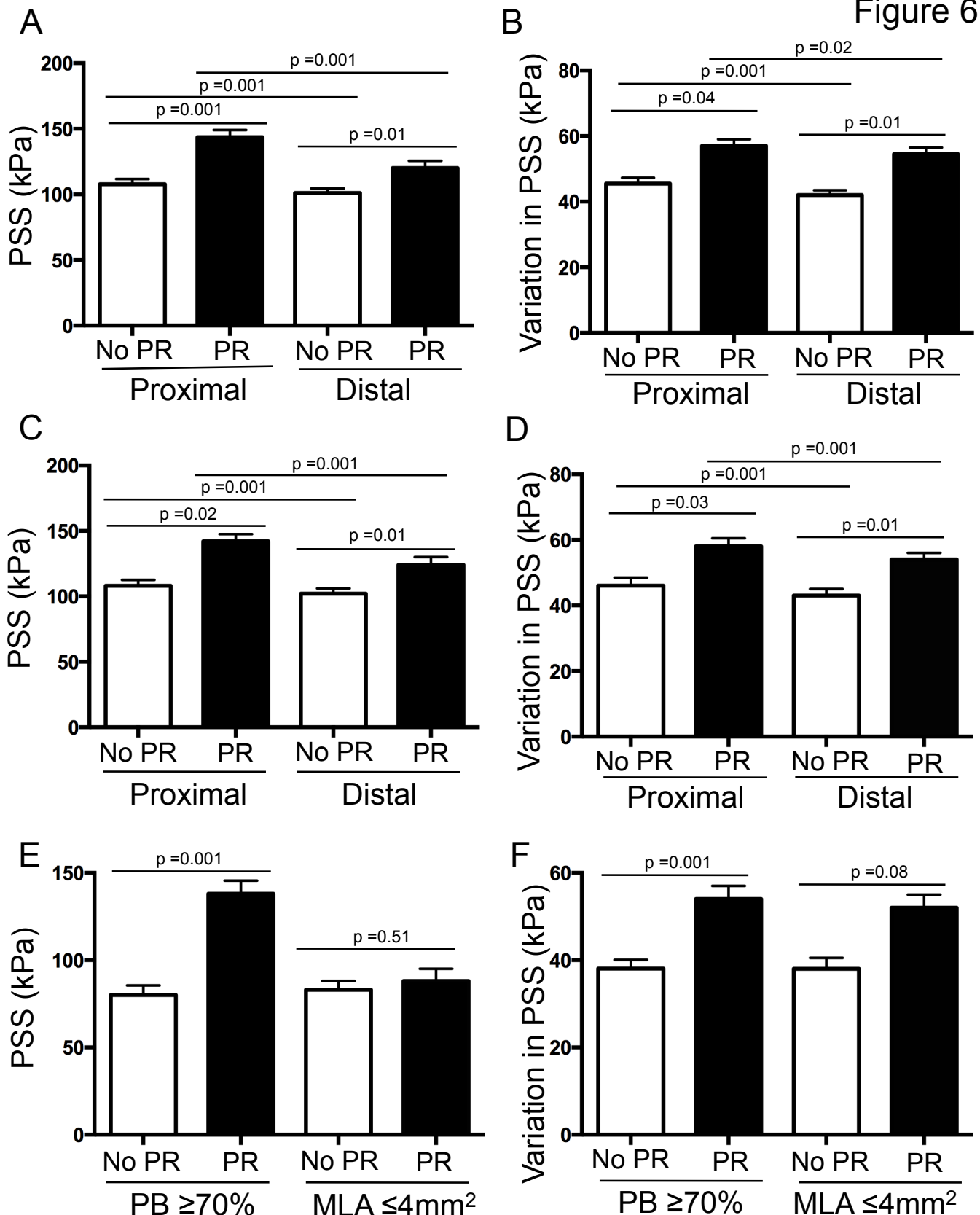


Figure 6. Plaque structural stress and variation in PSS in virtual-histology fibroatheromas with and without rupture

(A and B) PSS and variation in PSS in the proximal and distal segments of VH-FAs with and without plaque rupture. (C and D) PSS and variation in PSS in the proximal and distal segments of VH-TCFAs with and without PR. (E and F) PSS and variation in PSS in VH-TCFAs with PB ≥70% or MLA ≤4mm² with and without PR. MLA=minimal luminal area; PB=plaque burden; PR=plaque rupture; PSS=plaque structural stress; VH-FA=virtual-histology fibroatheroma; VH-TCFA=virtual-histology thin-cap fibroatheroma.

Figure 7

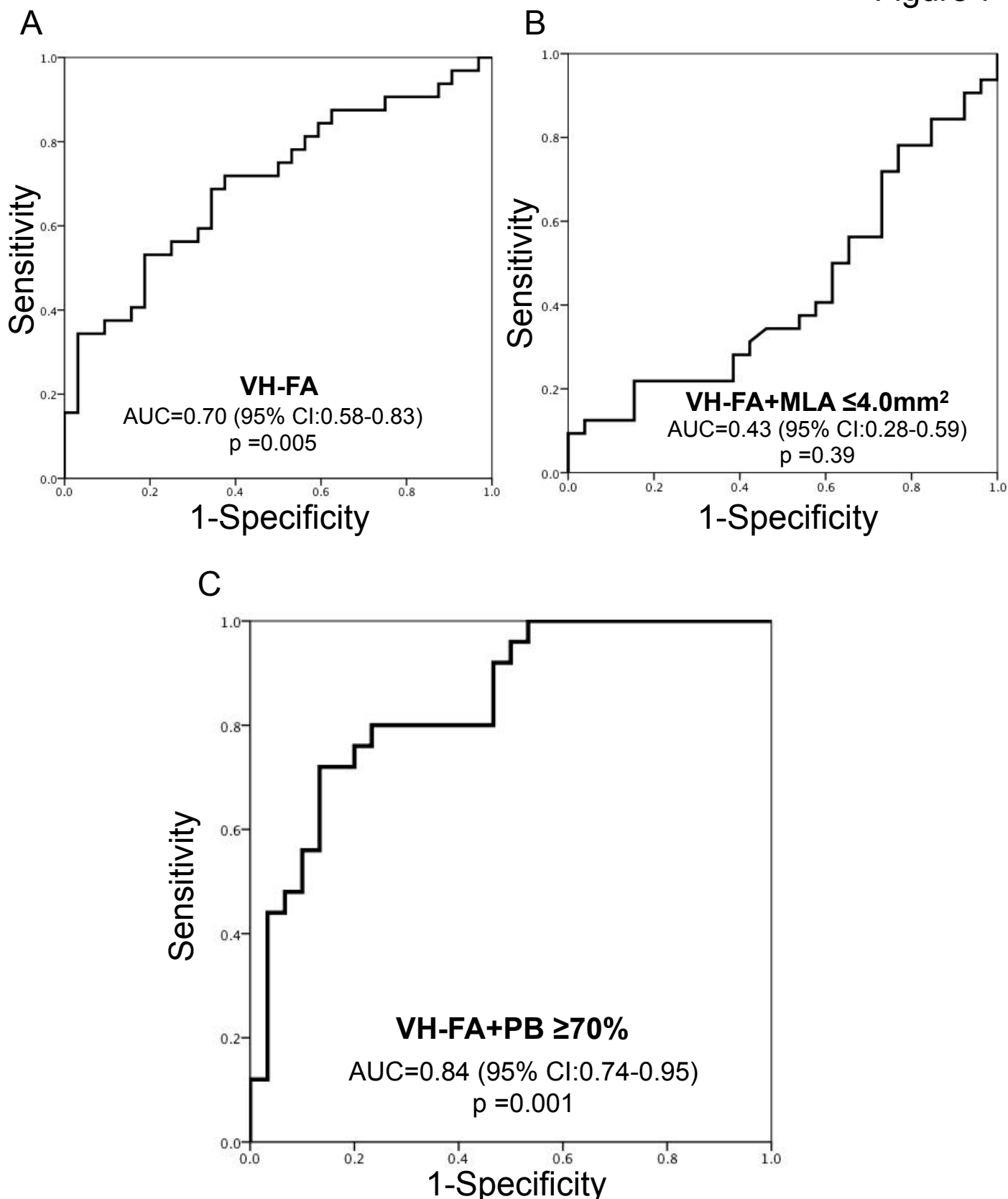


Figure 7. Receiver operating characteristic curves illustrating the discriminatory power of PSS to identify plaque rupture

(A) ROC curve for PSS in VH-FA **(B)** ROC curve for PSS in VH-FA+MLA $\leq 4\text{mm}^2$, and **(C)** ROC curve for PSS in VH-FA+PB $\geq 70\%$. AUC=area under the curve; CI=confidence interval; MLA=minimal lumen area; PB=plaque burden; ROC=receiver operating characteristic; VH-FA=virtual-histology fibroatheroma.